polymer papers

Development of molecular orientation in sequentially drawn PET films

J. B. Faisant de Champchesnel, D. I. Bower and I. M. Ward*
IRC in Polymer Science and Technology, University of Leeds, Leeds LS2 9JT, UK

and J. F. Tassin
Université du Maine, Faculté des Sciences, Laboratoire de Physicochimie Macromoléculaire, Avenue Olivier Messiaen, 72017 Le Mans Cedex, France

and G. Lorentz
Rhône-Poulenc Films, Magphane International, Saint Maurice de Beynost, BP140, 01701 Miribel Cedex, France
(Received 28 September 1992)

A study has been made of the transverse stretching of poly(ethylene terephthalate) film previously drawn longitudinally at constant force and width. The crystalline phase has been characterized using wide-angle X-ray diffraction: the orientation of the chain axis and the normal to the phenylene ring have been determined, as well as the crystallite size. Infra-red spectroscopy and refractive index measurements have been used to characterize the orientation of the material averaged over the crystalline and amorphous phases. The results showed that the crystals, which were preferentially aligned with their chain axes along the first stretching (longitudinal) direction, break down during the second drawing and that recrystallization takes place to produce crystallites with their *c*-axes aligned along the transverse stretching direction. The observed increase in the tendency for the normal to the phenylene ring to be normal to the film plane correlates with the increase in crystallite size along the chain axis for crystallites oriented with their chain axes in the transverse direction.

(Keywords: molecular orientation; PET films; infra-red spectroscopy; X-ray diffraction)

INTRODUCTION

Companies manufacturing plastic films have, for many years, shown a great interest in improving and controlling the mechanical properties in the plane of the film by increasing the orientation of the chain axes towards the plane of the film. In the case of poly(ethylene terephthalate) (PET) film, the industrial process is divided into three stages; the first stage is longitudinal drawing at constant force and constant width, in the second stage the film is stretched transversely at constant speed and constant width, and the third stage involves the thermosetting of the film.

In the past 20 years, many studies of the uniaxial and uniaxial–planar stretching of PET films have been carried out[1–4]. A fairly good understanding of the longitudinal stretching has therefore been reached. Far fewer studies have been done on transverse stretching[5–7]. The aim of this paper is to give further insight into the structural changes occurring in both the crystalline and the amorphous phase during the transverse stretching. The orientation in the crystalline phase and the crystallite size have been measured using wide-angle X-ray diffraction. The overall orientation in the material (amorphous and crystalline phases) has been determined using refractive indices and infra-red spectroscopy.

* To whom correspondence should be addressed

MATERIALS

The PET films used were biaxially oriented, sequentially drawn films. The first drawing was carried out by Rhône Poulenc on a pilot plant drawing machine, at a draw ratio λ_1 of 3.4 and a temperature of 127°C. The film was stretched at constant width and constant force between two rolls: a slow one (speed of the film = 0.167 m s^{-1}) and a fast one (speed = 0.567 m s^{-1}).

Four samples were cut from this one-way drawn 50 μm thick film. One (40 × 50 mm) was used to analyse the monodrawn material. The other three (48 × 100 mm, 33 × 100 mm, 25 × 100 mm) were drawn transversely to the first drawing direction on a specially designed drawing machine at the Saint Fons Research Centre of Rhône Poulenc; the width normal to the second draw direction was kept constant at 100 mm. In order to bring the sample from the ambient to the stretching temperature without significantly modifying the structure of the one-way drawn material, the following preheating programme was applied to each sample before stretching: 30 s heating at 87°C followed by 2 s heating at 120°C. The sample with an initial length of 48 mm along the second draw direction was drawn to a draw ratio $\lambda_2 = 2.2$, that of length 33 mm to $\lambda_2 = 3.6$ and that of length 25 mm to $\lambda_2 = 4.5$. The temperature was kept constant at 120°C and the film draw speed at 12 mm s^{-1}. The initial and final strain rates are shown in *Table 1*.

0032-3861/93/183763-08

Table 1 Sample details

Second draw ratio, λ_2	Strain rate $\dot{\varepsilon}$ (s^{-1})		Refractive indices			Density, d ($g\,cm^{-3}$)	Crystallinity, χ (%)
	initial	final	n_3	n_1	n_2		
1.0			1.6320	1.5765	1.5550	1.3616	22.2
2.2	0.300	0.136	1.6274	1.6260	1.5264	1.3719	30.1
3.6	0.520	0.144	1.6215	1.6445	1.5180	1.3745	32.9
4.5	0.583	0.130	1.6059	1.6745	1.4989	1.3716	30.5

GENERAL THEORETICAL BACKGROUND

The function that describes the distribution of orientations of the structural units in a biaxially oriented polymer may be written in the form[2,8]:

$$N(\theta, \phi, \psi) = \sum P_{lmn} Z_{lmn}(\cos\theta) e^{-im\phi} e^{-in\psi} \quad (1)$$

where θ, ϕ, ψ are the Euler angles relating axes fixed within each unit to the symmetry axes fixed in the sample and $N(\theta, \phi, \psi) \sin\theta\, d\theta\, d\phi\, d\psi$ is the fraction of units whose axes lie in the generalized solid angle $\sin\theta\, d\theta\, d\phi\, d\psi$. The expansion is in terms of generalized spherical harmonics with coefficients P_{lmn}. Infra-red (i.r.) spectroscopy and refractive index measurements can give information only about the coefficients P_{lmn} for $l=2$ and m or $n=0$ or 2, i.e. P_{200}, P_{202}, P_{220} and P_{222}. The coefficient P_{200} is the well known average over the second-order Legendre polynomial $\langle P_2(\cos\theta)\rangle = \frac{1}{2}(3\langle\cos^2\theta\rangle - 1)$ where θ is the angle between the chain axis and the principal symmetry axis chosen in the sample, which is usually the draw direction in a uniaxially or one-way drawn sample. The coefficient P_{220} is a measure of the departure from uniaxial symmetry of the chain axis distribution and is zero for true uniaxial symmetry. The coefficient P_{202} is zero if there is no preferred orientation of the chains around their own axes and the coefficient P_{222} is zero if either the sample is uniaxial or there is no preferred orientation of the chains around their own axes.

In the present paper OX_3 is chosen parallel to the first drawing (or machine) direction, OX_1 parallel to the transverse direction and OX_2 parallel to the normal to the film. It is often useful to choose different orientations of the notional set of axes fixed within the sample and of the notional set of axes fixed within the unit that are used in defining the P_{lmn}. If the principal reference axes used for defining the Euler angles are OX_3 within the sample and Ox_3 within the unit, as is assumed in reference 2, we shall label the P_{2mn} as $P_{2mn}^{3/3}$. In general $P_{2mn}^{i/j}$ will mean that Ox_i has been chosen as the reference axis in the unit and OX_j as the reference axis in the sample and the remaining reference axes in both sets have been cyclically permuted. It may then be shown, for example, that:

$$P_{202}^{2/i} = \tfrac{1}{6}(2P_{200}^{3/i} + P_{200}^{2/i}) \quad (2)$$

and

$$P_{220}^{i/3} = \tfrac{1}{6}(2P_{200}^{i/1} + P_{200}^{i/3}) \quad (3)$$

EXPERIMENTAL

X-ray diffraction

To investigate the distribution of orientations of the crystallites, X-ray data were obtained for two reflections:

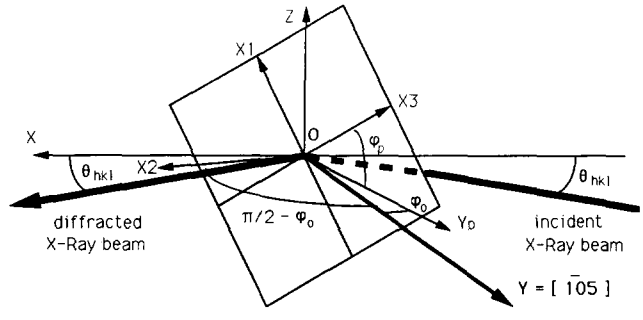

Figure 1 X-ray experiment in transmission (axes and angles are defined in the text)

$(\bar{1}\,0\,5)$ (plane normal close to the chain axis) and (1 0 0) (plane normal close to the normal to the phenylene ring). A Huber wide-angle X-ray diffractometer was used.

$(\bar{1}\,0\,5)$ reflection. The $(\bar{1}\,0\,5)$ reflection was studied in transmission; the experimental procedure is shown in *Figure 1*. $OXYZ$ is a set of orthogonal axes fixed with respect to the diffractometer. θ_{hkl} for $hkl = \bar{1}\,0\,5$ is the angle at which the diffraction from the $(\bar{1}\,0\,5)$ planes is maximum on a 2θ scan. The incident and the refracted beams are situated in the OXY plane, θ_{hkl} being the angle between the incident beam and OX. The normal to the film lies in the OXY plane, φ_o is the angle between OX and the normal to the film and φ_p is the angle between OX_3 (machine direction in the plane of the film) and OY_p, where OY_p is the line of intersection of the film plane and the plane OXY. The angle φ_p may be varied by rotating the film about its normal.

To collect the data, the following procedure was used. The angle φ_o was chosen and φ_p was varied from 0° to 180° in steps of 3°. For $\varphi_o > 20°$, the intensity becomes very weak and independent of φ_p at a given value of φ_o. Data were therefore stored for φ_o taking values every 5° from 0° up to 20°. Scans were made at $2\theta_{\bar{1}05} = 43.0°$ for the one-way drawn sample and at $2\theta_{\bar{1}05} = 43.2°$ for the other samples. An intensity matrix $I(\varphi_p, \varphi_o)$ resulted which had to be corrected for amorphous background, and for changes of absorption with φ_o as described below.

The values of the orientation averages $P_{200}^{\bar{1}05i}$ with respect to machine direction (OX_3), transverse direction (OX_1) and normal direction (OX_2) were calculated using the following formulae:

$$P_{200}^{\bar{1}05/3} = \tfrac{1}{2}(3\langle\cos^2(\bar{1}\,0\,5, OX_3)\rangle - 1) \quad (4a)$$

$$P_{200}^{\bar{1}05/1} = \tfrac{1}{2}(3\langle\cos^2(\bar{1}\,0\,5, OX_1)\rangle - 1) \quad (4b)$$

$$P_{200}^{\bar{1}05/2} = -(P_{200}^{\bar{1}05/3} + P_{200}^{\bar{1}05/1}) \quad (4c)$$

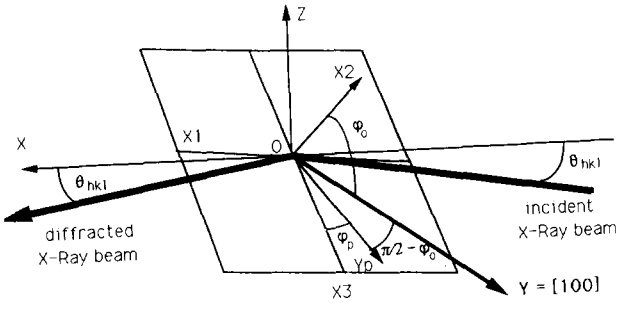

Figure 2 X-ray experiment in reflection (axes and angles are defined in the text)

where

$$\langle\cos^2(\bar{1}\,0\,5, OX_3)\rangle = \frac{\int_{\varphi_p}\int_{\varphi_o} I_c(\varphi_p, \varphi_o)\cos^2\varphi_p \cos^3\varphi_o \,d\varphi_p\, d\varphi_o}{\int_{\varphi_p}\int_{\varphi_o} I_c(\varphi_p, \varphi_o)\cos\varphi_o \,d\varphi_p\, d\varphi_o} \tag{5a}$$

$$\langle\cos^2(\bar{1}\,0\,5, OX_1)\rangle = \frac{\int_{\varphi_p}\int_{\varphi_o} I_c(\varphi_p, \varphi_o)\sin^2\varphi_p \cos^3\varphi_o \,d\varphi_p\, d\varphi_o}{\int_{\varphi_p}\int_{\varphi_o} I_c(\varphi_p, \varphi_o)\cos\varphi_o \,d\varphi_p\, d\varphi_o} \tag{5b}$$

The integrations were carried out by using a subroutine which fits the digitized, corrected $I_c(\varphi_p, \varphi_o)$ function and integrates it once fitted, where I_c is the corrected intensity.

(1 0 0) reflection. A reflection procedure was used to study the (1 0 0) reflection and is displayed in *Figure 2*. $OXYZ$ is the same set of orthogonal axes as before and the normal to the film (OX_2) lies in the OYZ plane. θ_{100} is the angle at which the diffraction from (1 0 0) is close to the maximum on the 2θ scan. The maximum is at $2\theta_{100} \simeq 25.5°$ but a slightly larger value for $2\theta_{100}$ was chosen to minimize overlap with $(1\,\bar{1}\,0)$; $2\theta_{100}$ was set at 26.0° for the four samples. The incident and refracted beams lie in the OXY plane, θ_{100} being the angle between the incident beam and OX. OY_p is the line of intersection of the OYZ plane and the plane of the film. The angle φ_o is the angle OYX_2. The angle φ_p is the angle between OY_p and the machine direction, OX_3.

To collect the data, the following procedure was used: φ_p was first chosen and φ_o was varied from 0° to 50° in steps of 2°. Values of φ_p were chosen in steps of 15° from 0° to 90°. The result of these measurements is a matrix $I(\varphi_o, \varphi_p)$ with φ_o from 0° to 50°. For $\varphi_o > 50°$ the intensity was taken to be zero (see below). The intensity matrix $I(\varphi_o, \varphi_p)$ was corrected for changes of absorption with φ_o and for the amorphous background as described below.

The values of $P_{200}^{100/i}$ with respect to the machine direction (OX_3), the transverse direction (OX_1), the normal direction (OX_2) were calculated by using expressions similar to equation (4) with

$$\langle\cos^2(1\,0\,0, OX_2)\rangle = \frac{\int_{\varphi_p}\int_{\varphi_o} I_c(\varphi_o, \varphi_p)\cos^2\varphi_o \sin\varphi_o \,d\varphi_p\, d\varphi_o}{\int_{\varphi_p}\int_{\varphi_o} I_c(\varphi_o, \varphi_p)\sin\varphi_o \,d\varphi_p\, d\varphi_o} \tag{6a}$$

$$\langle\cos^2(1\,0\,0, OX_1)\rangle = \frac{\int_{\varphi_p}\int_{\varphi_o} I_c(\varphi_o, \varphi_p)\sin^2\varphi_p \sin^3\varphi_o \,d\varphi_p\, d\varphi_o}{\int_{\varphi_p}\int_{\varphi_o} I_c(\varphi_o, \varphi_p)\sin\varphi_o \,d\varphi_p\, d\varphi_o} \tag{6b}$$

The integrations were performed in the same way as for the $(\bar{1}\,0\,5)$ reflection.

Corrections to the X-ray data

(i) Choice of the baseline in the (φ_o, φ_p)-scans. In order to make a simple and reliable choice of the baseline, we tried to ensure that it was the same for the 2θ scans and the (φ_o, φ_p) scans.

(a) In transmission for $(\bar{1}\,0\,5)$ reflection. *Figure 3* shows (φ_o, φ_p) and 2θ scans for a highly one-way drawn sample. On the (φ_o, φ_p) scan, $\varphi_p = 0$ represents the machine

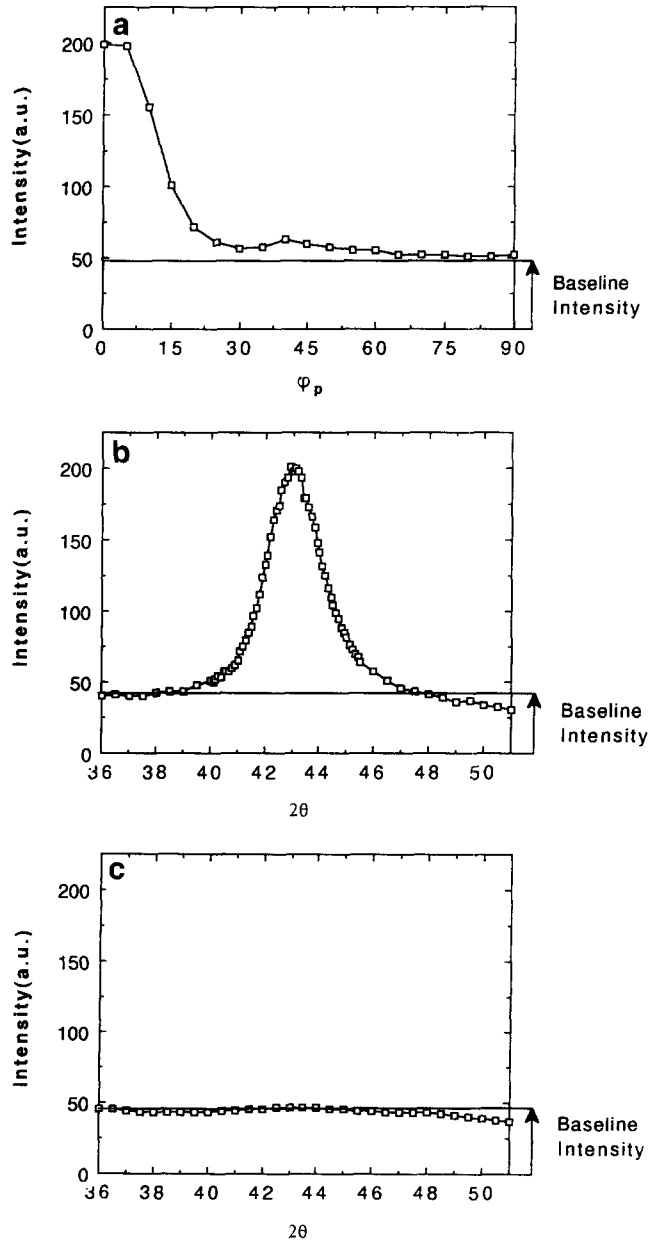

Figure 3 Choice of the baseline for the $(\bar{1}\,0\,5)$ reflection (not all data points are shown; a.u. = arbitrary units). (a) Scattered intensity *versus* φ_p at $\varphi_o = 0°$; (b) scattered intensity *versus* 2θ at $\varphi_p = 0°$ and $\varphi_o = 0°$; (c) scattered intensity *versus* 2θ at $\varphi_p = 90°$ and $\varphi_o = 0°$

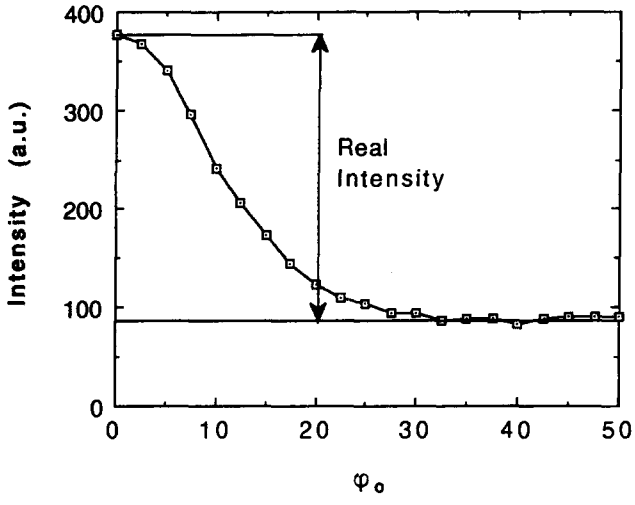

Figure 4 Choice of the baseline for the (1 0 0) reflection (not all data points are shown), scattered intensity *versus* φ_o at $2\theta = 26°$

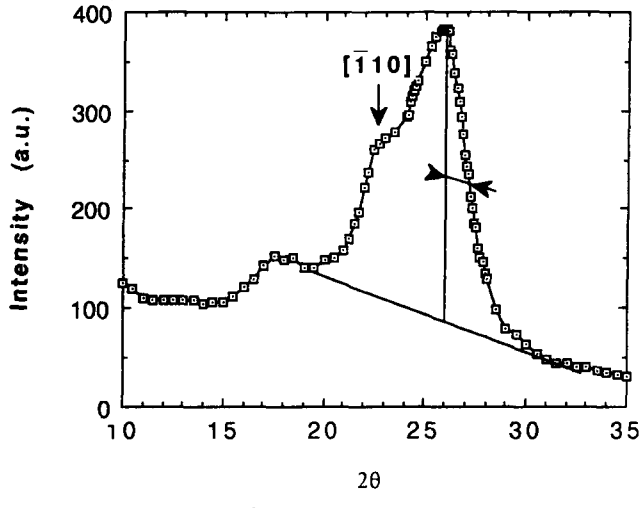

Figure 5 Measurement of the crystallite size along [1 0 0] (not all data points are shown)

direction whereas $\varphi_p = 90°$ represents the transverse direction (*Figure 3a*).

In *Figure 3c*, it can be clearly seen that there are no crystallites with [1̄ 0 5] directions oriented along the transverse direction ($\varphi_p = 90°$). The scattered intensity is almost constant from $2\theta = 36°$ to $2\theta = 43°$ and falls only slightly above $2\theta = 45°$. The same intensity is also observed at $2\theta = 36°$ for $\varphi_o = 0°$ (*Figure 3b*) and for $\varphi_p = 90°$ in *Figure 3a* (where $2\theta = 43°$). This common value was assumed to be the background value.

(*b*) *In reflection for (1 0 0).* A typical (φ_o) scan is displayed in *Figure 4* which shows that it is possible to deduce the baseline from the lower level of intensity of this scan. This matches quite well the baseline chosen on the 2θ scan to measure the crystallite size (see *Figure 5* and below).

(*ii*) *Correction for absorption.* When (φ_o, φ_p) scans are performed, the irradiated volume of the sample varies with φ_o. Part of the incident beam is also absorbed by the sample. These two phenomena must be taken into account. (φ_o, φ_p) scans were performed in transmission (for the (1̄ 0 5) reflection) and in reflection (for the (1 0 0) reflection) and the correction factor is different for these two geometries[9].

The absorption coefficient μ can be calculated from atomic absorption coefficients and also determined experimentally. Close agreement was found between experimental and calculated values, namely 9.183 and $9.156 \times 10^{-4}\ \mu m^{-1}$, respectively. The value $\mu = 9.156 \times 10^{-4}\ \mu m^{-1}$ was used in the corrections, which were found to be small for both scattering geometries.

Measurement of the crystallite size

The crystallite size was measured from the angular broadening of the diffraction peaks using the Debye–Scherrer formula[9]:

$$L_{hkl} = \frac{\lambda}{(\Delta\theta_{1/2}^2 - \Delta\theta_{inst}^2)^{1/2}} \frac{1}{\cos\theta_{hkl}} \qquad (7)$$

in which λ is the wavelength of the X-rays (= 1.542 Å), θ_{hkl} is the angle at which the intensity is maximum on the 2θ scan and $\Delta\theta_{inst}$ is the instrumental broadening.

L_{T05}. The measurements of crystallite size along [1̄ 0 5] were made in the transmission mode (*Figure 1*) with φ_o set at 0°. For measurement of crystallite size along [1̄ 0 5] in the machine or transverse direction, φ_p was set at 0° or 90°, respectively. The angle 2θ was varied from 36° to 51°. The same baseline as that previously defined was chosen. It consists in drawing an horizontal line from $2\theta = 36°$ on the 2θ scan (*Figure 3b*). It is also possible to draw a slightly sloping line from $2\theta = 36°$ to $2\theta = 51°$ (*Figure 6*). The difference between the values of $L_{\bar{1}05}$ determined using the two ways of choosing the baseline is less than the uncertainty (< 6%) calculated by differentiation of expression[7] and insertion of the experimental uncertainty in $\Delta\theta_{1/2}$ of 0.1°.

L_{100}. The measurements of the crystallite size along [1 0 0] were made in the reflection geometry (*Figure 2*). φ_o was set at 0°; φ_p was arbitrarily set at 0°. The baseline shown in *Figure 5* is consistent with the previous one. Owing to the overlap with the [1̄ 1 0] reflection at small angles, only half of $\Delta\theta_{1/2}$ was directly measured on the 2θ scans, as shown in *Figure 5*. The uncertainty in L_{100} is less than 4%, corresponding to an experimental uncertainty of 0.1° in $\Delta\theta_{1/2}$.

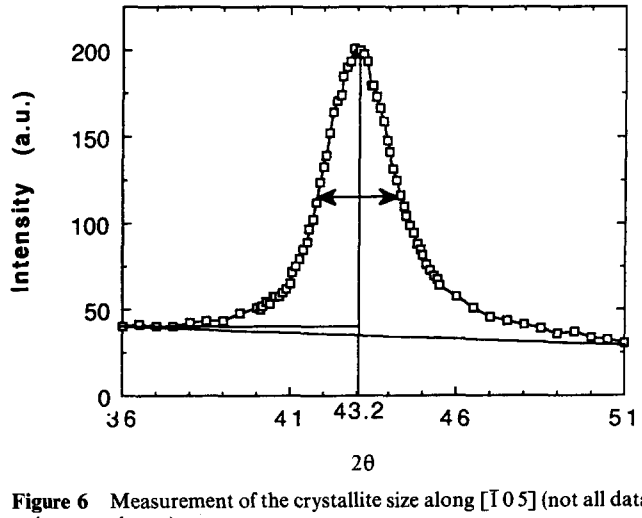

Figure 6 Measurement of the crystallite size along [1̄ 0 5] (not all data points are shown)

Refractive indices

The refractive indices of the samples were measured in the three principal directions using a BS-60 Abbe refractometer, and their values are shown in *Table 1*.

Density d and crystallinity χ were calculated from the mean refractive index $\bar{n}=(n_1+n_2+n_3)/3$ by the following formulae[10]:

$$d=4.047\frac{n^2-1}{n^2+2}(\mathrm{g\,cm^{-3}}) \tag{8}$$

$$\chi=(d-d_a)/(d_c-d_a) \tag{9}$$

where d_a is the density of the amorphous phase and d_c is the density of the crystalline phase. These were taken to be 1.335 and 1.455 g cm^{-3}, respectively[10].

The refractive indices of the sample may be used to deduce information about the orientation of the phenylene ring normals, provided that the molecular polarizabilities are known. In order to calculate the molecular polarizabilities, orthogonal axes $Ox_1x_2x_3$ within the repeat unit were chosen as follows: Ox_3 is parallel to the chain axis direction, Ox_1 is normal to Ox_3 and in the plane of the ring, Ox_2 is normal to Ox_1 and Ox_3. Ox_2 is then close to the normal to the ring. The choice of the numerical values of the principal molecular polarizabilities α_i ($i=1, 2, 3$) will be discussed below.

The orientation has been calculated using the following relationships[2]:

$$A_2=\frac{\phi_2-(\phi_1+\phi_3)/2}{\phi_1+\phi_2+\phi_3}=\Delta P_{200}^{2/2}+\delta P_{202}^{2/2} \tag{10}$$

$$B_2=\frac{\phi_3-\phi_1}{\phi_1+\phi_2+\phi_3}=4\Delta P_{220}^{2/2}+\frac{2\delta}{3}P_{222}^{2/2} \tag{11}$$

where

$$\Delta=\frac{\alpha_2-(\alpha_1+\alpha_3)/2}{\alpha_1+\alpha_2+\alpha_3}\qquad \delta=\frac{\alpha_3-\alpha_1}{(\alpha_1+\alpha_2+\alpha_3)/3} \tag{12}$$

$$\text{and } \phi_i=\frac{n_i^2-1}{n_i^2+2} \text{ for } i=1, 2 \text{ or } 3. \tag{13}$$

Infra-red measurements

The i.r. measurements were carried out on a Nicolet 740 *FT*i.r. spectrometer, and data between 700 and 1100 cm^{-1} were analysed. Two regions were studied, ~1020 cm^{-1} and ~875 cm^{-1}, to provide information about the orientation of the chain axis and the normal to the phenylene ring, respectively[2].

The absorption at 1020 cm^{-1} corresponds to the vibration shown in *Figure 7a*. The dipole moment is close to the C_1–C_4 axis in the phenylene ring and so this vibration gives information about the orientation of the chain axis. The observed absorption peak can be decomposed into two components[2], one at 1021 cm^{-1} and one at 1018 cm^{-1}. The absorption at 875 cm^{-1} corresponds to a vibration of the phenylene ring for which the transition dipole moment is approximately normal to the ring (see *Figure 7b*). The observed absorption peak can be decomposed into two components[2], one at 877 cm^{-1} and one at 873 cm^{-1}.

The experimental procedure is described in detail in reference 2. A curve-fitting program was used to find the position, width (full width at half-maximum absorbance) and intensity of each (Lorentzian) peak. For each sample, each of the four required spectra was fitted separately and then the positions and the widths were averaged for each peak. Four new curve fits with positions and widths set at these average values were then carried out, with only the intensity allowed to vary.

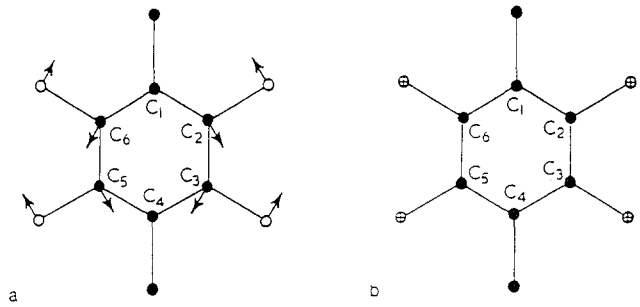

Figure 7 Approximate modes of the vibration assigned to the i.r. absorption peaks at: (a) 1017 cm^{-1}; (b) 875 cm^{-1}

The value of $P_{200}^{2/2}$ can be calculated from the data for the 875 cm^{-1} absorption using the expression[2]

$$P_{200}^{2/2}=\frac{\Phi_2-(\Phi_1+\Phi_3)/2}{\Phi_1+\Phi_2+\Phi_3} \tag{14}$$

where

$$\Phi_i=6n_ik_i/(n_i^2+2)^2 \tag{15}$$

and n_i and k_i are respectively the real and imaginary parts of the refractive index for radiation polarized parallel to OX_i.

Similar equations can be used for calculating $P_{200}^{2/3}$ and $P_{200}^{2/1}$. Equation (14) and its analogues can also be used to calculate the values of $P_{200}^{p/1}$, $P_{200}^{p/2}$, $P_{200}^{p/3}$ but using Φ values calculated from the data for the 1020 cm^{-1} absorption, where p stands for the C_1–C_4 direction in the ring.

RESULTS

Crystallinity

As shown in *Table 1*, there seems to be a slight change in crystallinity from the one-way drawn sample ($\chi=22\%$) to the sequentially drawn sample ($\chi=30\%$). This slight increase may be due to the 2 s preheating programme at 120°C that was applied to the sequentially drawn samples; for those samples, the crystallinity remains almost independent of the draw ratio.

Orientation in the crystalline phase. The normal to the ($\bar{1}$ 0 5) plane is approximately parallel to the chain axis (c-axis), the angle between these two directions being 9.8°. Similarly, the normal to the (1 0 0) plane is approximately normal to the phenylene ring, the angle between these two directions being 19°. As a first approximation, these deviations from the chain axis and phenylene ring normal directions will be neglected.

(*a*) *Chain axis distribution.* The values of $P_{200}^{\bar{1}05/i}$ found by the procedures described above are displayed in *Figure 8*. The problem of the background is an important issue; the higher the isotropic background subtracted from $I(\phi_o, \phi_p)$, the higher is the calculated value of $|P_{200}^{\bar{1}05/i}|$. The uncertainty in the value of $P_{200}^{\bar{1}05/i}$ caused by uncertainty in the background was taken to be that corresponding to the change produced when a constant amount equal to ±5% of the maximum intensity value was added to all $I_c(\phi_o, \phi_p)$ values. These uncertainties are

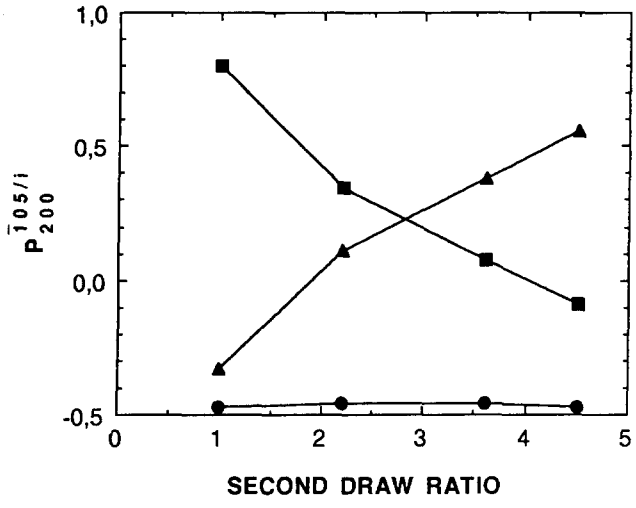

Figure 8 Second moment $P_{200}^{\bar{1}05/i}$ *versus* the second draw ratio with respect to: (■) the machine direction ($i=3$); (▲) the transverse direction ($i=1$); (●) the normal direction ($i=2$)

Table 2 The values of $P_{200}^{\bar{1}05/i}$ and $P_{200}^{100/i}$ and their uncertainties

Second draw ratio	Reference axis i of the sample[a]	$P_{200}^{\bar{1}05/i}$	$P_{200}^{100/i}$
	3	0.80 ± 0.17	-0.42 ± 0.05
1.0	1	-0.33 ± 0.16	0.01 ± 0.01
	2	-0.47 ± 0.01	0.41 ± 0.05
	3	0.35 ± 0.02	-0.44 ± 0.04
2.2	1	0.11 ± 0.02	-0.31 ± 0.01
	2	-0.46 ± 0.01	0.75 ± 0.06
	3	0.08 ± 0.02	-0.37 ± 0.05
3.6	1	0.38 ± 0.02	-0.43 ± 0.06
	2	-0.46 ± 0.01	0.80 ± 0.12
	3	-0.09 ± 0.10	-0.34 ± 0.05
4.5	1	0.56 ± 0.11	-0.44 ± 0.05
	2	-0.47 ± 0.01	0.78 ± 0.10

[a] 3, machine; 1, transverse; 2, normal

shown in *Table 2*. Whichever background is used, it appears that the chain axes remain close to the plane of the film during the second drawing, since $P_{200}^{\bar{1}05/2} < -0.4$. As $P_{200}^{\bar{1}05/3}$ falls, $P_{200}^{105/1}$ increases; loss of orientation towards the machine direction (OX_3) is compensated by the increase in orientation towards the transverse direction (OX_1).

(*b*) *Distribution of the normal to the phenylene ring.* Once again, the influence of the background is quite strong. The trend of $P_{200}^{100/i}$ values is displayed in *Figure 9* with values calculated as described earlier. The effect of a change of background equal to $\pm5\%$ of the maximum peak height is displayed in *Table 2*. The most significant effect of the second drawing is that the normal to the phenylene ring becomes more closely aligned towards the normal to the plane of the sample (OX_2), as shown by the large increase in $P_{200}^{100/2}$. Most of the increase is compensated by a fall in $P_{200}^{100/1}$ and there is only a small change in the alignment with respect to the machine direction (OX_3).

Crystallite size. $L_{\bar{1}05}$: As the second draw ratio is increased the crystallite size parallel to the chain axis falls along the machine direction while it increases along the transverse direction (*Figure 10*). Along the machine direction, the crystallite size decreases from four unit cells to three unit cells on average whereas it increases up to five unit cells along the transverse direction.

L_{100}: Along the [100] direction there is a noticeable increase of the crystallite size (from four to six unit cells as an average) (*Figure 11*).

Overall orientation of the normal to the phenylene ring. The overall orientation of the normal to the phenylene ring can be obtained from refractive indices or i.r. data.

The values of $P_{200}^{2/i}$ deduced from the i.r. measurements at 875 cm^{-1} are displayed in *Table 3*. The uncertainties have been determined from the variability of the parameters in the curve-fitting procedure. Equations (10) and (11) cannot be used directly to obtain values of $P_{200}^{2/i}$, since these equations involve too many unknowns.

It can, however, be shown that $|P_{202}^{2/2}| < \frac{1}{6}(1-P_{200}^{2/2})$. From equation (10), we then deduce that:

$$\frac{6A_2+\delta}{6\Delta+\delta} < P_{200}^{2/2} < \frac{6A_2-\delta}{6\Delta-\delta} \qquad (16)$$

By cyclic permutation of indices it follows that

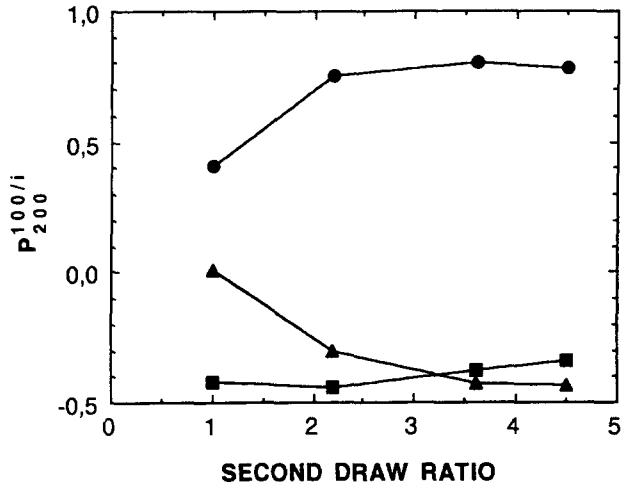

Figure 9 Second moment $P_{200}^{100/i}$ *versus* the second draw ratio with respect to: (■) the machine direction ($i=3$); (▲) the transverse direction ($i=1$); (●) the normal direction ($i=2$)

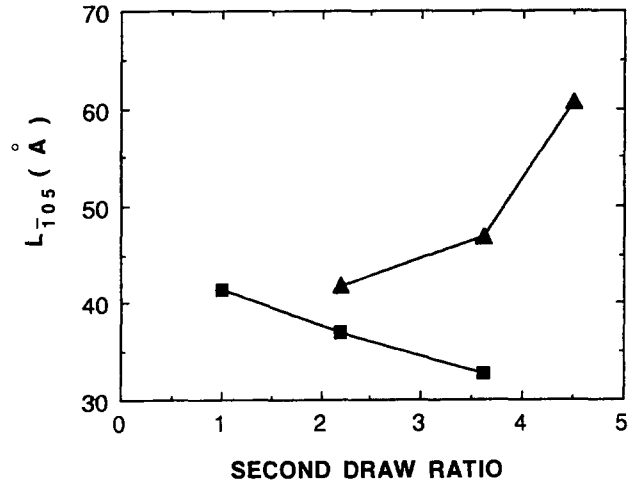

Figure 10 Crystallite size along [$\bar{1}$05] *versus* the second draw ratio with respect to: (■) the machine direction ($i=3$); (▲) the transverse direction ($i=1$)

equation (16) holds for $i=1$, 2 or 3 if $P_{200}^{2/2}$ is replaced by $P_{200}^{2/i}$ and A_2 by A_i, where A_1 and A_3 are obtained from A_2 by cyclically permuting the indices on the ϕ_i. The limits on the values of $P_{200}^{2/1}$, $P_{200}^{2/2}$ and $P_{200}^{2/3}$ are not independent, however, since the sum of these three quantities must be zero.

Equation (16) gives the extreme limits on the values of the quantities $P_{200}^{2/i}$ if the quantities $P_{202}^{2/i}$ are unknown. For any real distribution of orientations it is unlikely that these limits will be approached, and the uncertainties in the quantities $P_{200}^{2/i}$ calculated by assuming that $\delta P_{202}^{2/i}$ is zero are therefore taken to be one-half of those given by the limits. The values of $P_{200}^{2/i}$ and the uncertainties calculated in this way are given in *Table 4*.

In calculating these values the molecular polarizabilities given by Jarvis *et al.*[2] for their model A have been used. If other values in the literature corresponding essentially to model A are used[11,12], the values of $P_{200}^{2/i}$ obtained do not differ from those given in the table by more than the uncertainties. If the polarizabilities given by Jarvis *et al.* for their model B are used, the values of $P_{200}^{2/i}$ are all numerically higher by $\sim 30\%$ and the uncertainties are very much larger.

Equation (2) shows that $P_{202}^{2/i}$ can be calculated from the quantities $P_{200}^{3/i}$ and $P_{200}^{2/i}$, which can be determined by i.r. spectroscopy, as described above. The errors made in calculating $P_{200}^{2/i}$ from equation (10) by assuming that $\delta P_{202}^{2/i}$ is zero can thus be calculated, assuming that the refractive indices and the i.r. intensities are indeed determined by the same units. These errors (or corrections) are also shown in *Table 4* and are seen to be smaller than the uncertainties quoted, which are therefore justified as reasonable uncertainties on the basis of refractive index data alone.

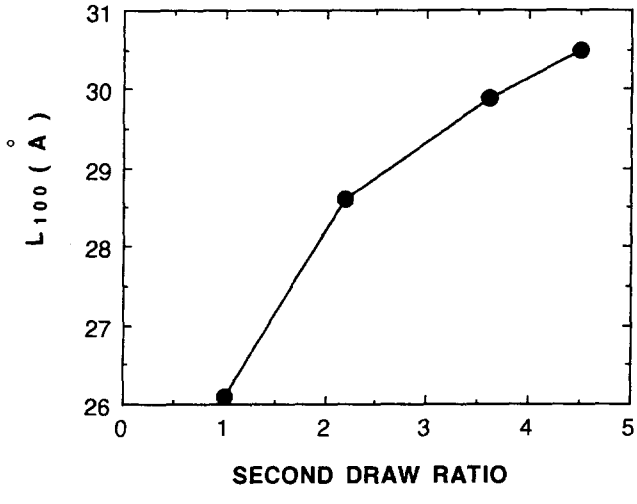

Figure 11 Crystallite size along [1 0 0] *versus* the second draw ratio

DISCUSSION

Crystallite orientation and crystallite size

The X-ray (φ_o, φ_p) scans showed that as the transverse stretching progressed, the concentration of chain axes along the machine direction reduced, and that the only direction where the chain axes were reappearing was close to the transverse direction. 2θ scans showed a fall of the crystallite size $L_{\bar{1}05}$ along the machine direction and a rise of the crystallite size along the transverse direction.

These two pieces of experimental evidence – the number of chain axes along the machine direction and the transverse direction and changes in crystallite size – lead to the following conclusions:

1. The reduction of the crystallite size along the machine direction indicates that the larger crystallites are destroyed or reduced in size as the transverse draw ratio is increased.
2. New crystallites form along the transverse direction as a result of the realignment of chains during the transverse drawing process, giving birth to a second family of chain axes.

Overall orientation from refractive indices and i.r.

There is fairly good agreement between the values for the overall orientation obtained from refractive indices

Table 3 Overall orientation averages from infra-red data

Second draw ratio, λ_2	1020 cm^{-1}			875 cm^{-1}		
	$P_{200}^{p/1}$	$P_{200}^{p/2}$	$P_{200}^{p/3}$	$P_{200}^{2/1}$	$P_{200}^{2/2}$	$P_{200}^{2/3}$
1.0	Sat.	Sat.	Sat.	Sat.	Sat.	Sat.
2.2	Sat.	Sat.	Sat.	-0.15 ± 0.03	0.31 ± 0.06	-0.16 ± 0.03
3.6	0.22 ± 0.02	-0.28 ± 0.03	0.06 ± 0.01	-0.16 ± 0.02	0.26 ± 0.03	-0.10 ± 0.01
4.5	0.31 ± 0.03	-0.28 ± 0.03	-0.03 ± 0.01	-0.24 ± 0.02	0.32 ± 0.03	-0.08 ± 0.01

Sat., saturated

Table 4 Overall orientation averages from refractive index data

Second draw ratio, λ_2	$P_{200}^{2/1}$	Correction from i.r.	$P_{200}^{2/2}$	Correction from i.r.	$P_{200}^{2/3}$	Correction from i.r.
1.0	0.04 ± 0.02		0.13 ± 0.02		-0.17 ± 0.03	
2.2	-0.13 ± 0.03		0.26 ± 0.02		-0.13 ± 0.03	
3.6	-0.20 ± 0.03	0.013	0.31 ± 0.02	0.014	-0.11 ± 0.03	0.001
4.5	-0.31 ± 0.03	0.017	0.37 ± 0.01	0.011	-0.06 ± 0.02	0.007

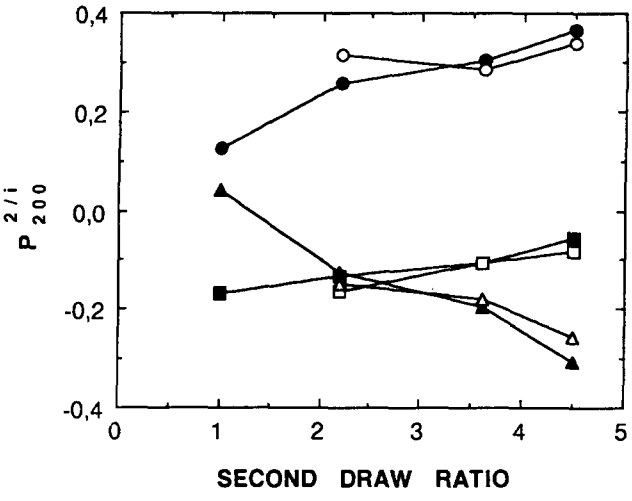

Figure 12 Second moment $P_{200}^{2/i}$ of the phenylene ring *versus* the second draw ratio with respect to: (■) the machine direction ($i=3$) from refractive indices; (▲) the transverse direction ($i=1$) from refractive indices; (●) the normal direction ($i=2$) from refractive indices; (□) the machine direction ($i=3$) from i.r.; (△) the transverse direction ($i=1$) from i.r.; (○) the normal direction ($i=2$) from i.r.

and i.r. measurements (see *Figure 12*). Any differences could be explained by two factors.

One is the uncertainty in the calculation of the $P_{200}^{2/i}$ from refractive indices; this uncertainty is greater for $P_{200}^{2/1}$ and $P_{200}^{2/3}$ than for $P_{200}^{2/2}$ and applies to all second draw ratios.

Another possible causes of differences is the magnitude of the absorbances in the i.r. data. The reliability of i.r. data is strongly dependent on the absorbance of the peak concerned. For the sample with a second draw ratio of 1 (one-way drawn sample), the absorbance peaks are saturated and no calculation of $P_{200}^{2/i}$ can be made from i.r. data. For the sample with a second draw ratio of 2.2, a strong absorbance (up to 2.3) is observed and the value of $P_{200}^{2/2}$ is therefore not very reliable.

For the samples with higher second draw ratios (3.6 and 4.5), the absorbances remain lower than 1.4 and the i.r. data are therefore more reliable: $P_{200}^{2/2}$ from refractive indices and i.r. data are in good agreement, and the differences for $P_{200}^{2/3}$ and $P_{200}^{2/1}$ may be due as much to uncertainties in the values deduced from the refractive indices as to those in the i.r. results.

The trends observed by i.r. spectroscopy for the overall chain orientation are qualitatively similar to those observed from the X-ray diffraction measurements of the ($\bar{1}$ 0 5) reflection, although it must be emphasized that the C_1–C_4 direction in the benzene ring makes an angle of about 17° with the ($\bar{1}$ 0 5) plane normal. In spite of this difference in detail between the i.r. and X-ray measurements it is still possible to conclude that the overall orientation is less than the crystallite orientation, which can be understood on the reasonable assumption that the amorphous regions are less well oriented than the crystalline regions.

Similar considerations apply to the i.r. measurements of the orientation of the benzene ring plane normal, which makes an angle of 19° with the (1 0 0) plane normal. Although the i.r. measurements of the overall plane normal orientations are qualitatively similar to those obtained by X-ray diffraction for the (1 0 0) plane normal, it can be concluded that the orientation of the crystalline regions is greater than the overall orientation.

CONCLUSIONS

The development of the orientation of the chain axis and the normal to the phenylene ring has been fully characterized for the second drawing process of sequentially drawn PET films.

The two main features of this second drawing process are (1) the breakdown of crystallites oriented with their *c*-axes close to the machine direction and the formation of new crystallites with their *c*-axes oriented close to the transverse direction and (2) an increase in the orientation of the phenylene ring plane normals with respect to the film plane normal.

These results suggest that as the orientation of the molecular network is transformed by the second drawing process to give the predominant molecular orientation in the second draw direction, the crystallites originally formed in the machine direction break down and a new generation of crystallites is formed with their *c*-axes in the transverse direction by nucleation and growth of crystalites in what is now the primary direction.

In a further publication it is proposed to consider the influence of the initial crystallite size and the temperature of the second drawing process on the final structure of these biaxially oriented films.

ACKNOWLEDGEMENTS

The authors are grateful to J. Beautemps (Societé Rhône Poulenc) and Dr A. P. Unwin for help with X-ray measurements and Professor L. Monnerie for fruitful discussions.

REFERENCES

1 Kashiwagi, M., Cunningham, A., Manuel, A. J. and Ward, I. M. *Polymer* 1973, **14**, 111
2 Jarvis, D. A., Hutchinson, I. J., Bower, D. I. and Ward, I. M. *Polymer* 1980, **21**, 41
3 LeBourvellec, G., Monnerie, L. and Jarry, J. P. *Polymer* 1986, **27**, 856
4 Lapersonne, Ph., Tassin, J. F., Monnerie, L. and Beautemps, J. *Polymer* 1991, **32**, 3331
5 Yoshihara, N., Fukushima, A., Watanabe, Y., Nakai, A., Nomura, S. and Kawai, H. *Sen-i Gakkaishi* 1981, **37**, 387
6 Cakmak, M., Spruiell, J. E. and White, J. L. *Polym. Eng. Sci.* 1987, **27**, 893
7 Cakmak, M., Spruiell, J. E. and White, J. L. *Polym. Eng. Sci.* 1989, **29**, 1534
8 Roe, R. J. *J. Appl. Phys.* 1964, **36**, 2025
9 Alexander, L. E. 'X-ray Diffraction Methods in Polymer Science', Wiley-Interscience, New York, 1969
10 DeVries, A. J., Bonnebat, C. and Beautemps, J. *J. Polym. Sci.* 1977, **58**, 109
11 Pinnock, P. R. and Ward, I. M. *Br. J. Appl. Phys.* 1964, **15**, 1559
12 Kurigama, I., Tomiita, K. and Shirakashi, K. *Sen-i Gakkaishi* 1964, **20**, 431